AIAA JOURNAL
Vol. 38, No. 10, October 2000

Coupled Helicopter Rotor/Flexible Fuselage Aeroelastic Model for Control of Structural Response

Richard C. Cribbs,* Peretz P. Friedmann,† and Thiem Chiu‡
University of California, Los Angeles, Los Angeles, California 90095-1597

A refined coupled rotor/flexible fuselage aeroelastic response model is developed for vibration reduction studies based on active control of structural response (ACSR). The structural model is capable of representing flexible, hingeless rotors combined with a flexible fuselage, and a rigid platform combined with the actuators required for modeling the ACSR system and is combined with a free wake model. The influence of rotor/fuselage coupling and improved aerodynamics on the vibratory hub loads is investigated.

Nomenclature

A	= beam cross-sectional area
a_{N_bC}, a_{N_bS}	= cosine and sine parts of acceleration at various fuselage locations
a_z	= fuselage vertical acceleration at various locations
C_{d_0}	= blade drag coefficient
C_O, C_I, C_{NW}	= matrices of induced velocity influence coefficients
C_W	= helicopter coefficient of weight
c	= blade chord
$\boldsymbol{D}$	= wake distortion
E	= Young's modulus of elasticity
EI_y, EI_z	= blade bending stiffnesses in flap and lead-lag
$\boldsymbol{F}_b^A$, $\boldsymbol{F}_b^G$, $\boldsymbol{F}_b^I$	= blade aerodynamic, gravitational, and inertial forces
$\boldsymbol{F}_{b_0}$, $\boldsymbol{F}_{b_{\mathrm{nc}}}$, $\boldsymbol{F}_{b_{\mathrm{ns}}}$	= Fourier coefficients of blade equations of motion
$\boldsymbol{F}_{e_0}$, $\boldsymbol{F}_{e_{\mathrm{nc}}}$, $\boldsymbol{F}_{e_{\mathrm{ns}}}$	= Fourier coefficients of elastic fuselage equations of motion
$\boldsymbol{F}_{\mathrm{fus}}$	= total fuselage forces
F_{N_bC}, F_{N_bS}	= cosine and sine parts of rotor hub forces
$\boldsymbol{F}_{r_0}$, $\boldsymbol{F}_{r_{\mathrm{nc}}}$, $\boldsymbol{F}_{r_{\mathrm{ns}}}$	= Fourier coefficients of fuselage rigid body equations of motion
F_T, M_T	= tail rotor thrust and moment
F_x, F_y, F_z	= vibratory hub shear components
F_0, M_0	= constant part of rotor hub loads
fC_{df}	= fuselage equivalent flat plate drag area
GJ	= blade torsional stiffness
$[I]$	= fuselage inertia tensor
I_p	= polar moment of inertia
I_x, I_y, I_z	= fuselage beam cross-sectional principal moment of inertia
J	= beam torsional constant
L	= Lagrangian
M	= fuselage total mass
$\boldsymbol{M}_b^A$, $\boldsymbol{M}_b^G$, $\boldsymbol{M}_b^I$	= blade aerodynamic, gravitational, and inertial moment
$\boldsymbol{M}_{\mathrm{fus}}$	= total fuselage moments
M_{N_bC}, M_{N_bS}	= cosine and sine parts of hub moments
M_{ns}	= nonstructural consistent mass matrix
M_x, M_y, M_z	= vibratory hub moment components
m_b	= blade mass distribution per unit length
N	= matrix of shape functions for calculation of nonstructural mass matrix
N_b	= number of blades
N_H, N_{el}, N_{rg}	= number of harmonics retained in Fourier expansion of blade, fuselage elastic, and rigid body degrees of freedom
Q_i	= fuselage generalized force
$\boldsymbol{q}$	= response vector
$\boldsymbol{q}_b$, $\boldsymbol{q}_e$, $\boldsymbol{q}_r$	= vectors of blade, fuselage elastic, and rigid body degrees of freedom
$\boldsymbol{q}_{b_0}$, $\boldsymbol{q}_{b_{\mathrm{nc}}}$, $\boldsymbol{q}_{b_{\mathrm{ns}}}$	= Fourier coefficients of blade response
$\boldsymbol{q}_{e_0}$, $\boldsymbol{q}_{e_{\mathrm{nc}}}$, $\boldsymbol{q}_{e_{\mathrm{ns}}}$	= Fourier coefficients of fuselage elastic response
$\boldsymbol{q}_{r_0}$, $\boldsymbol{q}_{r_{\mathrm{nc}}}$, $\boldsymbol{q}_{r_{\mathrm{ns}}}$	= Fourier coefficients of fuselage rigid body response
R	= rotor radius
R_x, R_y, R_z	= fuselage rigid body translational degrees of freedom
$\boldsymbol{R}_0$	= fuselage center of mass position in inertial frame
$\boldsymbol{r}_b$	= position of rotor blade point
$\boldsymbol{r}_w$	= position of wake element
$\boldsymbol{r}_0$	= undeformed position of fuselage point with respect to the fuselage center of mass in fuselage reference frame
$\boldsymbol{r}'$	= deformation of fuselage point in fuselage reference frame
T	= kinetic energy
U_e	= elastic strain energy
u, v, w	= blade displacements in axial, chordwise, and flapwise directions, respectively
V	= volume of integration
x	= blade spanwise coordinate
α_R	= rotor trim pitch angle
β_p	= blade precone angle
Γ_I, Γ_O	= inboard and outboard circulation peaks defining the strength of the tip vortices
Γ_{ij}	= bound vorticity at azimuth j and spanwise location i
γ	= Lock number
$\delta(\,)/\delta t$	= time derivative relative to fuselage local coordinates
ε	= nondimensional parameter representing order of magnitude of typical blade slopes
θ_G	= geometric pitch angle
θ_{tr}	= tail rotor collective pitch angle
θ_x, θ_y, θ_z	= fuselage rigid body rotational degrees of freedom
θ_0, θ_{1c}, θ_{1s}	= blade collective pitch, cyclic cosine and sine pitch angles, respectively
λ	= nondimensional induced velocity
μ	= advance ratio
$\boldsymbol{\xi}$	= vector of modal participations
ξ_i	= normal coordinates for truncated fuselage modal matrix
ρ	= mass density

Received 16 February 1999; revision received 16 February 2000; accepted for publication 28 March 2000.

*Ph.D. Candidate, Mechanical and Aerospace Engineering Department; currently Research Fellow, University of Michigan, Ann Arbor, MI 48109-2140.

†Professor, Mechanical and Aerospace Engineering Department; currently Francois-Xavier Bagnoud Professor, Department of Aerospace Engineering, University of Michigan, Ann Arbor, MI 48109-2140. Fellow AIAA.

‡Postdoctoral Scholar, Mechanical and Aerospace Engineering Department. Member AIAA.

ρ_A = air density
ρ_M = equivalent density function for nonstructural mass representation
σ = rotor solidity ratio
Φ = matrix of fuselage mode shapes
Φ_{AC} = modal matrix of actuator displacements
ϕ = blade elastic twist angle
ϕ_s = rotor trim roll angle
ψ = blade azimuth angle or nondimensional time ($=\Omega t$)
Ω = angular speed of rotor
ω = angular velocity of fuselage frame relative to inertial frame
ω_{F_i}, ω_{L_i}, ω_{T_i} = the ith rotating blade flap, lag, and torsional frequencies

Introduction

REDUCTION of vibration levels in helicopters below acceptable limits is one of the central problems facing rotorcraft designers. Increasing demands for expanding the flight envelope, such as nap of earth flying, high speed and high g maneuvers, coupled with the need to improve system reliability and reduce maintenance costs, have resulted in more stringent vibration control standards. The adoption of ADS-27 by the U.S. Army illustrates the increased emphasis placed on the development of rotorcraft with drastically reduced vibration levels.[1,2] There has been a steady decrease in rotorcraft vibration levels over the years. However, with the adoption of stringent vibration control requirements for the next generation helicopters, further reduction in vibration levels below 0.05 g, or even 0.02 g, will be needed. Therefore, a substantial body of research and development effort has been directed toward vibration prediction and reduction methodologies in helicopters.[3–5] A detailed summary of the NASA/ARMY contributions to rotorcraft vibration technology has been presented in Ref. 5.

The main rotor is one of the principal contributors to high vibration levels in the helicopter fuselage. Therefore, the geometry of the rotor system, the structural dynamic characteristics of the rotor blades, and the fuselage play significant roles in influencing vibrations in helicopters. The various schemes available for vibration reduction in helicopters can be classified as either passive or active.[3,4] This paper is concerned with active approaches to vibration reduction which have been reviewed in Ref. 6.

As described in Ref. 6, three active control approaches have received considerable attention during the last twenty-five years: higher harmonic control, where all of the blades are provided with the same pitch input through a conventional swashplate; individual blade control, in which each blade is given its own pitch input in the rotating reference frame; and the last approach, developed more recently, the actively controlled flap, where a partial span, trailing edge flap mounted on the blade is actively controlled in the rotating reference frame.

In 1986, a new approach to active control of vibrations emerged. This method is based on a somewhat broader concept of direct control of structural response.[7] This new approach, denoted by the term Active Control of Structural Response (ACSR), was initially developed by King and Staple.[7] It differs from the previous active control approaches because the vibration reduction is accomplished in the nonrotating system. The ACSR scheme is based on the idea that in a linear system one can superimpose two independent responses such that the total response is minimized. When applying this scheme to the helicopter vibration reduction problem, the fuselage is excited by controlled forcing inputs at selected locations so that the combined response of the fuselage, due to both the rotor loads and the applied excitations, is minimized. The schematic representation of such a coupled rotor/active control/fuselage dynamic system and its associated control system for vibration reduction is depicted in Figs. 1 and 2. In Fig. 1, a four-bladed coupled rotor/flexible fuselage model with four actuators for vibration suppression is shown. The ACSR platform is shown as the rectangular structure (plate 1) at the top of the fuselage. The actuators, depicted by the heavy (dark) vertical lines in Fig. 1, extend between points p_1–p_2, p_3–p_4, p_5–p_6, p_7–p_8, respectively, and are connected to the four corners

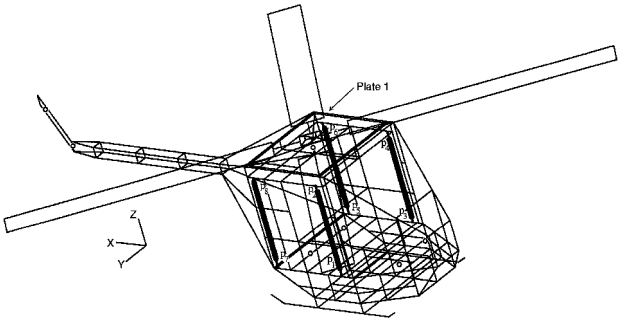

Fig. 1 Coupled rotor/fuselage dynamic system.

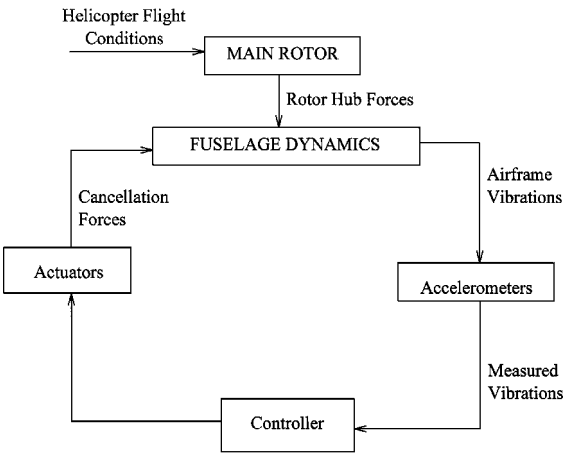

Fig. 2 Helicopter system schematic for ACSR.

of the ACSR platform. The schematic control loop governing the ACSR system is shown in Fig. 2.

Preliminary tests of the ACSR system have produced very promising results for the control of vibration in helicopters.[7–9] In the tests, the selection of sensors and actuators was based on results obtained from extensive ground shake tests. The major advantages of the ACSR system are 1) one can select locations for preferential reduction of vibratory motion, 2) reduced power requirements, and 3) minimal airworthiness requirements.[7]

The success of the ACSR system is evident from the fact that a version of this system is currently used for vibration reduction in one of the most modern helicopters being produced in Europe, the EH101. Furthermore, another variant of the ACSR system, the active vibration reduction (AVR) system, has recently been tested in both ground and flight tests.[10,11] In this approach, the gear-box is oscillated instead of an ACSR platform.

Despite the remarkable experimental successes of the ACSR system, an analytical model of such a complex combined rotor/actuator/fuselage dynamic system has not been considered in the literature before. Such an analytical model and the simulation capability that it provides is essential for the fundamental understanding and successful implementation of the ACSR approach. Such a model enables studies of optimal sensor locations (for vibration sensing) and force application points that increase the performance of the vibration reduction system.

The primary objective of this paper is to describe a new coupled rotor/flexible fuselage aeroelastic response model, including an ACSR platform and actuators required for the simulation of the ACSR system on a rotorcraft combined with a free wake model. The model consists of an N_b-bladed rotor with flexible hingeless blades, a free wake model, a finite element model for the flexible fuselage, and a set of four actuators located in fuselage capable of producing substantial oscillatory forces required for implementing the ACSR approach. The model is used to simulate the behavior of a four-bladed helicopter resembling an MBB BO-105 rotorcraft.

It is important to note that relatively few coupled rotor/flexible fuselage aeroelastic response models exist that are capable of modeling the vibration levels present in such a complicated

structural dynamic system. Most coupled rotor/fuselage models available combine a rotor with a number of flexible blades with the fuselage rigid body degrees of freedom, and the use of such models is aimed at studying the aeromechanical stability behavior in forward flight.[12,13] A few coupled rotor/flexible fuselage models exist in the literature. Typical of these is a model described in Ref. 14 that combines a flexible rotor with a flexible fuselage. The fuselage model was relatively simple, consisting of a flexible beam with bending flexibility in two mutually perpendicular planes and twist about the beam axis, but it lacked nonstructural masses and a realistic fuselage. Other studies have represented the coupled rotor/flexible fuselage model by a one-dimensional beam, where the beam itself is modeled using a number of discrete beam-type finite elements.[15,16] Again, the important role of nonstructural masses in accurately simulating the frequency content of the coupled rotor/flexible fuselage system was not addressed in Refs. 15 and 16. Other studies have shown remarkable differences in vibration levels in a coupled rotor/flexible fuselage system when using linear inflow and comparing it to free wake models. Loads obtained using a free wake model resulted in vibration levels that were 100 times higher than those obtained using a linear inflow model at certain advance ratios.[17,18] The fuselage model used in Refs. 17 and 18 consisted of a "stick" model of the AH-1G. Thus, none of these models are capable of simulating the refined local vibration levels needed for studying the ACSR system. The current paper remedies this situation by presenting an analytical simulation capability suitable for vibration reduction studies using ACSR, and it also makes a major contribution toward the development of a refined coupled rotor/flexible fuselage aeroelastic response modeling capability.

Mathematical Formulation

The coupled rotor/flexible fuselage model is capable of representing a rotor with flexible hingeless blades combined with a flexible fuselage, and four force actuators which are located at the corners of the fuselage cabin. The description of the model, given below, is separated into its components; namely, rotor, wake, fuselage, and ACSR platform and actuators. For active vibration reduction studies, the model described in this paper is combined with a control algorithm and sensors placed at specific fuselage locations.

Rotor Model

A fully flexible hingeless blade model with coupled flap-lag-torsional dynamics is used. The nonlinear partial differential equations describing the blade dynamics of an isolated rotor blade undergoing moderate deflections are given by Eqs. (5–7) of Ref. 19. The structural operator in these equations is independent of the hub motion, and the blade loads are left in a generic, symbolic form. This arrangement permits this blade model to be used in the current coupled rotor/flexible fuselage model with no modifications.

The distributed aerodynamic, gravitational, and inertial loads per unit length are symbolically derived and combined to obtain the total distributed force and moment acting on the blade. These loads, including the effects of fuselage motion, are derived using a symbolic manipulation program MACSYMA.[20]

The aerodynamic loads are obtained from Greenberg's quasi-steady aerodynamic theory,[21] whereas the inertial loads are based on D'Alembert's principle. Reverse flow is included, but stall and compressibility effects are neglected. The inextensional assumption for the axial deformation of the blade, commonly used in rotary-wing aeroelasticity, is employed to express the blade axial deformation in terms of its bending deformations.[12–14]

The inertial and aerodynamic loads are derived explicitly using an ordering scheme that allows one to have expressions of manageable size.[14,22,23] Such ordering schemes have been also used in other similar studies involving coupled rotor/flexible fuselage dynamics.[15,16] The ordering scheme is based on the assumption that

$$\mathcal{O}(1) + \mathcal{O}(\varepsilon^2) \cong \mathcal{O}(1) \tag{1}$$

where ε is a small dimensionless parameter on the order of a typical blade slope. Equation (1) implies that terms of the order ε^2 are negligible compared to unity.

The most significant quantities used in the formulation are assigned the following orders of magnitude:

$$\frac{\partial}{\partial x}, \frac{\partial}{\partial t}, \frac{\partial}{\partial \psi}, \mu, \cos(\psi), \sin(\psi) = \mathcal{O}(1)$$

$$\theta_G, \phi = \mathcal{O}\left(\varepsilon^{\frac{1}{2}}\right), \qquad u = \mathcal{O}(\varepsilon^2)$$

$$\frac{c}{R}, \lambda, \alpha_R, \frac{v}{R}, \frac{w}{R}, \frac{EI_z}{m_b\Omega^2R^4}, \frac{EI_y}{m_b\Omega^2R^4} = \mathcal{O}(\varepsilon)$$

$$\theta_x, \theta_y, \theta_z \frac{C_{d_0}}{a}, \frac{fC_{df}}{R^2}, R_x, R_y, R_z = \mathcal{O}\left(\varepsilon^{\frac{3}{2}}\right) \tag{2}$$

Such ordering schemes are based on experience and are applied carefully so as to retain all the important terms.[23] This ordering scheme is used to systematically eliminate the appropriate higher order nonlinear terms from the equations of motion.

Wake Model

The rotor wake model has been extracted from the comprehensive rotorcraft analysis tool, CAMRAD/JA,[24,25] and modified to be compatible with the aeroelastic response analysis employed in our simulation. The wake model is composed of a wake geometry model that determines the location of the wake in space and a wake calculation model that, given the wake geometry, calculates the induced velocity distribution.

The wake geometry scheme was developed by Scully.[26] Each wake element is created at the blade and is convected with the air's local velocity, which is composed of the free stream velocity and the wake induced velocity. The wake geometry is calculated as follows: 1) the positions of the blade generating the wake elements are calculated, 2) the undistorted wake is found by adding the contribution of the free stream velocity to the wake element creation points, and 3) the free wake geometry is found by adding the distortion due to the wake induced velocity to the undistorted geometry. A wake element is thus described by the position of the blade when the wake element was created and the time elapsed from the time of element creation to the current time. As illustrated in Fig. 3, the position of a generic wake element can therefore be described as

$$\boldsymbol{r}_w(\psi, \phi) = \boldsymbol{r}_b(\psi - \phi) + \phi \boldsymbol{v}_w + \boldsymbol{D}(\psi, \phi) \tag{3}$$

where ψ indicates the current blade azimuth position, ϕ is the nondimensional age of the wake element, and $\boldsymbol{v}_w$ is the freestream

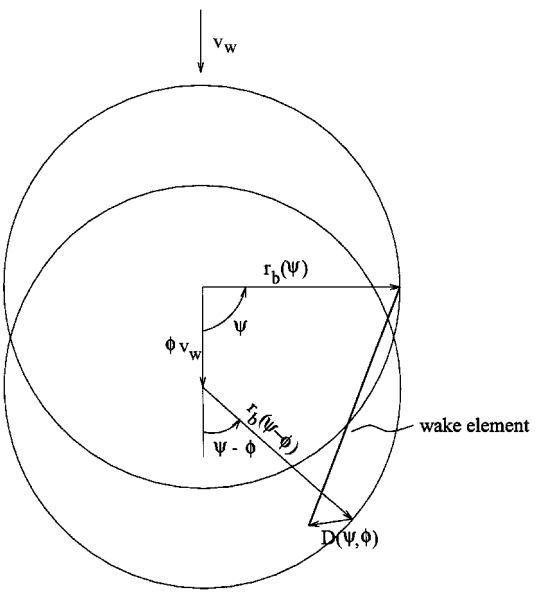

Fig. 3 Wake element.

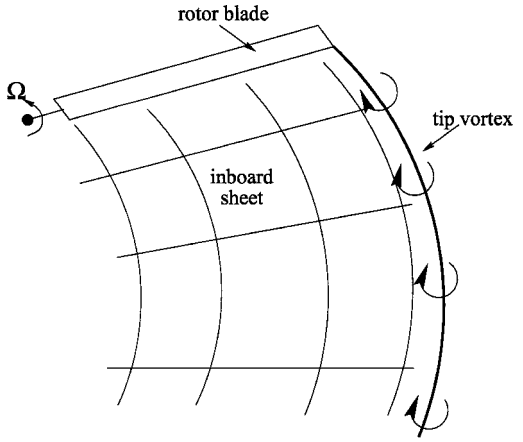

Fig. 4 Wake model.

velocity. The wake distortion $\boldsymbol{D}(\psi, \phi)$ is calculated by integrating in time the wake induced velocity acting on the wake element.

The wake calculation routine was developed by Johnson.[27] The model is based on a vortex lattice approximation of the wake consisting of two main elements: the tip vortex and an inboard vortex sheet as shown in Fig. 4. The tip vortex is a concentrated vorticity filament generated at the tip of the blade, whereas the inboard vortex sheet is due to trailed and shed vorticity and is much weaker and more diffuse than the tip vortex. The tip vortices are modeled as vortex lines with small viscous core radii, whereas the inboard sheet can be represented by either vortex sheet elements or vortex line segments with large core radii. Given the wake geometry and the bound circulation distribution, matrices of influence coefficients that describe the wake induced velocities as a function of blade bound circulations are calculated. A simple matrix multiplication of influence coefficients times the circulation distribution provides the induced velocities

$$\lambda_i = \sum_{j=1}^{J} \Gamma_{Oj} C_{Oj} + \sum_{j=1}^{J} \Gamma_{Ij} C_{Ij} + \sum_{j=0}^{K_{\mathrm{NW}}} \sum_{i=1}^{M} \Gamma_{ij} C_{\mathrm{NW}_{ij}} \tag{4}$$

where J and M are the numbers of azimuthal and spanwise stations, respectively, at which the induced velocities are calculated and K_{NW} is the number of azimuthal stations that describe the extent of the near wake.

Fuselage Model

The fuselage equations of motion are determined using a Lagrangian formulation. The position of each point on the fuselage is defined using two coordinate systems: a local coordinate system with its origin at the fuselage center of mass and an inertial reference system. The position of a point on the fuselage, denoted $\boldsymbol{R}$, can be described as a sum of the position of the center of mass in the inertial frame, $\boldsymbol{R}_0$, and the position of the specific fuselage point with respect to the center of mass in the local coordinate system $\boldsymbol{r}$ so that

$$\boldsymbol{R} = \boldsymbol{R}_0 + \boldsymbol{r} \tag{5}$$

The local position vector $\boldsymbol{r}$ is further broken down into undeformed position $\boldsymbol{r}_o$ and displacement due to elastic deformation $\boldsymbol{r}'$. Therefore, the overall position of a point on the fuselage is expressed as

$$\boldsymbol{R} = \boldsymbol{R}_0 + \boldsymbol{r}_0 + \boldsymbol{r}' \tag{6}$$

The velocity of a fuselage point with respect to the inertial frame is

$$\frac{\mathrm{d}\boldsymbol{R}}{\mathrm{d}t} = \frac{\mathrm{d}\boldsymbol{R}_0}{\mathrm{d}t} + \frac{\delta \boldsymbol{r}_0}{\delta t} + \frac{\delta \boldsymbol{r}'}{\delta t} + \boldsymbol{\omega} \times \boldsymbol{r} \tag{7}$$

Noting that $\delta \boldsymbol{r}_0 / \delta t = 0$, the kinetic energy of the fuselage is

$$T = \frac{1}{2} \int_V \left\{ \frac{\mathrm{d}\boldsymbol{R}_0}{\mathrm{d}t} \cdot \frac{\mathrm{d}\boldsymbol{R}_0}{\mathrm{d}t} + 2 \frac{\mathrm{d}\boldsymbol{R}_0}{\mathrm{d}t} \cdot \frac{\delta \boldsymbol{r}'}{\delta t} + \frac{\delta \boldsymbol{r}'}{\delta t} \cdot \frac{\delta \boldsymbol{r}'}{\delta t} + 2 \frac{\delta \boldsymbol{r}'}{\delta t} \cdot (\boldsymbol{\omega} \times \boldsymbol{r}) + (\boldsymbol{\omega} \times \boldsymbol{r}) \cdot (\boldsymbol{\omega} \times \boldsymbol{r}) + 2(\boldsymbol{\omega} \times \boldsymbol{r}) \cdot \frac{\mathrm{d}\boldsymbol{R}_0}{\mathrm{d}t} \right\} \rho \, \mathrm{d}V \tag{8}$$

The term

$$\int_V (\boldsymbol{\omega} \times \boldsymbol{r}) \cdot (\boldsymbol{\omega} \times \boldsymbol{r}) \rho \, \mathrm{d}V$$

is more commonly seen in the form $\boldsymbol{\omega}^T [I] \boldsymbol{\omega}$. In general, the inertia tensor is time varying due to elastic deformation, but, in this analysis, it will be assumed to be constant (i.e., the variance due to elastic deformation is assumed to be negligible).

For the local coordinate system, mean axes[28,29] are chosen. Mean axes are defined such that the linear and angular momenta due to elastic deformation are identically zero at every instant. It is assumed that the elastic deformation $\boldsymbol{r}'$ is small or that the displacement and rate are collinear. The mean axes constraints are satisfied if the natural modes are orthogonal to the rigid body translational and rotational modes.

Using mean axes and time-invariant densities, many terms in Eq. (8) are identically zero so that the kinetic energy is shown to be

$$T = \frac{1}{2} M \frac{\mathrm{d}\boldsymbol{R}_0}{\mathrm{d}t} \cdot \frac{\mathrm{d}\boldsymbol{R}_0}{\mathrm{d}t} + \frac{1}{2} \boldsymbol{\omega}^T [I] \boldsymbol{\omega} + \frac{1}{2} \int_V \frac{\delta \boldsymbol{r}'}{\delta t} \cdot \frac{\delta \boldsymbol{r}'}{\delta t} \rho \, \mathrm{d}V \tag{9}$$

Thus the kinetic energy of the fuselage is decoupled into strictly rigid body contributions,

$$\frac{1}{2} M \frac{\mathrm{d}\boldsymbol{R}_0}{\mathrm{d}t} \cdot \frac{\mathrm{d}\boldsymbol{R}_0}{\mathrm{d}t} + \frac{1}{2} \boldsymbol{\omega}^T [I] \boldsymbol{\omega}$$

and strictly elastic deformation contribution,

$$\frac{1}{2} \int_V \frac{\delta \boldsymbol{r}'}{\delta t} \cdot \frac{\delta \boldsymbol{r}'}{\delta t} \rho \, \mathrm{d}V$$

Since the fuselage is modeled as an assemblage of finite elements, the elastic displacements are defined by a finite number of generalized coordinates $\boldsymbol{q}_e$. In typical notation, the kinetic energy due to elastic deformation and the elastic strain energy are rewritten as

$$\frac{1}{2} \int_V \frac{\delta \boldsymbol{r}'}{\delta t} \cdot \frac{\delta \boldsymbol{r}'}{\delta t} \rho \, \mathrm{d}V = \frac{1}{2} \dot{\boldsymbol{q}}_e^T [M] \dot{\boldsymbol{q}}_e \tag{10}$$

$$U_e = \tfrac{1}{2} \boldsymbol{q}_e^T [K] \boldsymbol{q}_e \tag{11}$$

The equations of motion are determined using Lagrange's equation

$$\frac{\mathrm{d}}{\mathrm{d}t} \left(\frac{\partial L}{\partial \dot{q}_i} \right) - \frac{\partial L}{\partial q_i} = Q_i \tag{12}$$

The Lagrangian L is defined as

$$L = T - U = \frac{1}{2} M \frac{\mathrm{d}\boldsymbol{R}_0}{\mathrm{d}t} \cdot \frac{\mathrm{d}\boldsymbol{R}_0}{\mathrm{d}t} + \frac{1}{2} \boldsymbol{\omega}^T [I] \boldsymbol{\omega} + \frac{1}{2} \dot{\boldsymbol{q}}_e^T [M] \dot{\boldsymbol{q}}_e + \boldsymbol{g} \cdot \boldsymbol{R}_0 M - \frac{1}{2} \boldsymbol{q}_e^T [K] \boldsymbol{q}_e \tag{13}$$

It is easily seen that the Lagrangian is decoupled into terms due to rigid fuselage motion and terms due to the elastic deformation. Since the generalized coordinates, q_i, are also decoupled into terms defined by the motion of the center of mass and terms defined by the elastic displacement, $\boldsymbol{q}_e$, the equations of motion are decoupled into rigid body equations of motion and elastic fuselage equations of motion. The rigid body equations of motion are well known and are as follows:

$$M \ddot{\boldsymbol{x}}_{\mathrm{cm}} = \Sigma \boldsymbol{F} \tag{14}$$

where $\boldsymbol{F}$ includes all external forces applied to the body including the gravitational force, and

$$[I]\frac{\delta\boldsymbol{\omega}}{\delta t} + \boldsymbol{\omega} \times [I]\boldsymbol{\omega} = \Sigma \boldsymbol{M}_{\text{cm}} \tag{15}$$

where $\boldsymbol{M}_{\text{cm}}$ is the total moment about the center of mass due to external forces.

The elastic equations become

$$[M]\ddot{\boldsymbol{q}}_e + [K]\boldsymbol{q}_e = Q \tag{16}$$

The generalized forces are determined from the principal of virtual work[30]

$$Q_i = \frac{\partial}{\partial(\delta q_i)}(\delta W) \tag{17}$$

where δW is the virtual work associated with δq_i, the arbitrary virtual displacements of the generalized coordinates.

To determine the fuselage mass and stiffness matrices, the elastic fuselage is modeled as a three dimensional structure. A collection of elements (i.e., an element library) is used to generate the structural dynamic model of the fuselage. The elements used in the model consist of linear Euler–Bernoulli beams and nonstructural mass elements. To achieve a realistic structural dynamic model for the helicopter fuselage, it is important to account for the concentrated masses as shown by the open circles in Fig. 1. These nonstructural masses, such as fuel tanks, engine, transmission, payloads, etc., are modeled using a consistently derived finite element model.[31] Numerical results indicate that if concentrated masses are not properly accounted for in the fuselage model, the salient features of the first few modes corresponding to those present in an actual helicopter cannot be captured.[32] At each node, the nonstructural mass element is capable of three translational, as well as three rotational, degrees of freedom. The nonstructural consistent mass matrix is derived from the equation

$$M_{\text{ns}} = \int_0^l \int_A \rho_M N^T N \, \mathrm{d}A \, \mathrm{d}x \tag{18}$$

The nonstructural mass per unit length is modeled by an equivalent density function (ρ_M) defined over the length of the beam element l such that the product of ρ_M and the beam cross sectional area integrated over its length contributes an amount of mass equal to the nonstructural mass. Separate density functions are considered for axial, torsional, and bending dynamics. Analytical expressions for these equivalent density functions can be found in Ref. 31.

For the fuselage structure, Euler–Bernoulli beam elements are used. At each node, three translational and three rotational displacements in the x, y, z directions are used, for a total of twelve degrees of freedom for each beam. The interpolation of the torsional and axial displacements is linear, whereas cubic interpolation functions are used for the transverse bending displacements. The interpolation shape functions for the beam and truss elements, and the mass and stiffness matrices resulting from their implementation, can be found in Ref. 33.

Assembly of the individual finite elements into a global stiffness or mass matrix requires the transformation of the elemental degrees of freedom from a local coordinate system to a global coordinate system. The transformations and assembly are carried out in the usual manner. Once the global mass and stiffness matrices are obtained, the eigenvalue problem for the entire problem with 966 degrees of freedom is solved to obtain the frequencies and mode shapes of the fuselage. The solution is carried out using the International Mathematical and Statistical Library (IMSL) subroutine DGEGV.

Using a normal mode transformation, the fuselage mode shapes are used to describe the fuselage deformation. The generalized coordinates describing the fuselage elastic motion are expressed as

$$\boldsymbol{q}_e = \Phi\boldsymbol{\xi} \tag{19}$$

In the model, the fuselage dynamics are represented by a truncated set of eight natural modes of free vibration. This representation reduces the number of degrees of freedom associated with the fuselage flexibility while retaining the dominant components of fuselage deformation.

ACSR Platform and Actuators

An ACSR platform combined with its actuators is an important ingredient that has to be incorporated into the coupled rotor/flexible fuselage model, as shown in Fig. 1. In this study, the rotor system is mounted to a rigid rectangular plate connected to the fuselage. The engine and gear-box are assumed to be mounted to this rigid platform. Four actuators, represented by the heavy, dark vertical lines in Fig. 1, are connected between the four corners of the platform and separate locations within the fuselage. The corners of this plate are denoted p_2, p_4, p_6, and p_8. The actuators are aligned vertically and are connected to the bottom of the fuselage cabin at points p_1, p_3, p_5, and p_7. The locations of the actuator attachment points is somewhat arbitrary. The primary requirement is that there is relative motion between the actuator endpoints in the fuselage modes to be controlled by the ACSR system. The vertical alignment used in this study was chosen primarily to reduce the vertical accelerations in the fuselage cabin. No attempt was made to optimize the locations of the actuators.

The actuators are capable of producing small displacements, combined with substantial oscillatory forces. Oscillatory control inputs are sent to the actuators in order to counteract the rotor vibratory forcing and minimize vibrations in the fuselage. The actuator tip displacements are represented by

$$U_T(t) = \Phi_{\text{AC}}\boldsymbol{\xi}(t) \tag{20}$$

where $U_T(t)$ represents the total actuator tip displacements i.e., $U_T(t) = U_{\text{top}}(t) - U_{\text{bottom}}(t)$. The matrix Φ_{AC} denotes the modal matrix relating the actuator displacements in the physical and modal domains, with the vector $\boldsymbol{\xi}(t)$ representing the fuselage modal participation.

Solution Procedure

The solution of the coupled rotor/fuselage with free wake model proceeds in several nested iteration loops composed of a wake model loop, a coupled trim/aeroelastic response loop, and a blade circulation convergence loop. The outer loop is the wake loop and consists of three cases: 1) uniform inflow, 2) prescribed wake, and 3) free wake. In the uniform inflow case, no wake is used. The prescribed wake model uses the uniform inflow solution to define the wake geometry. There is no wake self-induced distortion in this iteration. The free wake uses the results from the prescribed wake to include the wake self-induced distortion. Several iterations of the free wake case are used to refine the solution.

Within each wake iteration, the coupled rotor/fuselage trim and aeroelastic response solutions are determined. In this study, the trim and response solutions are obtained simultaneously by satisfying the trim equilibrium and the vibratory response of the helicopter for all the rotor and fuselage degrees of freedom together. This coupled trim/aeroelastic response solution is obtained using the harmonic balance technique, which replaces a system of ordinary differential equations of motion in the time domain by a system of algebraic equations with constant coefficients in the frequency domain.[14,34] This transformation to the frequency domain is accomplished by performing Fourier series expansions on the various degrees of freedom present in the coupled rotor/flexible fuselage model. The equations of motion for the coupled rotor/fuselage system are concisely represented by

$$\boldsymbol{F}_b(\boldsymbol{q}, \dot{\boldsymbol{q}}, \ddot{\boldsymbol{q}}, \boldsymbol{q}_t; \psi) = 0 \tag{21}$$

$$\boldsymbol{F}_r(\boldsymbol{q}, \dot{\boldsymbol{q}}, \ddot{\boldsymbol{q}}, \boldsymbol{q}_t; \psi) = 0 \tag{22}$$

$$\boldsymbol{F}_e(\boldsymbol{q}, \dot{\boldsymbol{q}}, \ddot{\boldsymbol{q}}, \boldsymbol{q}_t; \psi) = 0 \tag{23}$$

$$\boldsymbol{F}_t(\boldsymbol{q}, \dot{\boldsymbol{q}}, \ddot{\boldsymbol{q}}, \boldsymbol{q}_t; \psi) = 0 \tag{24}$$

Equation (21) represents the blade flap-lag-torsional equations of motion. The vectors $\boldsymbol{F}_r$, $\boldsymbol{F}_e$, and $\boldsymbol{F}_t$ correspond to the fuselage

rigid body, the fuselage elastic motion expressed in modal domain, and the trim equations, respectively. The vector $\boldsymbol{q}_t$ represents the propulsive trim solution that consists of the quantities θ_0, θ_{1c}, θ_{1s}, θ_{tr}, α_R and ϕ_s. The response vector $\boldsymbol{q}$ consists of the blade, fuselage rigid body, and fuselage elastic degrees of freedom, i.e.,

$$\boldsymbol{q} = \{\boldsymbol{q}_b \quad \boldsymbol{q}_r \quad \boldsymbol{q}_e\}^T \tag{25}$$

The vector $\boldsymbol{q}_b$ represents the blade response in flap, lag, and torsion, i.e.,

$$\boldsymbol{q}_b = \{w \quad v \quad \phi\}^T \tag{26}$$

The system of coupled partial differential blade equations of motion is transformed to a system of ordinary nonlinear differential equations by applying Galerkin's method to eliminate the spatial variable. The blade degrees of freedom are approximated by two torsional, two lead-lag, and three flap, uncoupled, free vibration modes of a rotating cantilevered blade.

The vector $\boldsymbol{q}_r$ represents the fuselage rigid body translational and rotational responses, i.e.,

$$\boldsymbol{q}_r = \{R_x \quad R_y \quad R_z \quad \theta_x \quad \theta_y \quad \theta_z\}^T \tag{27}$$

The vector $\boldsymbol{q}_e$ represents the fuselage elastic deformations, i.e.,

$$\boldsymbol{q}_e = \Phi\{\xi_1 \quad \ldots \quad \xi_n\}^T \tag{28}$$

where n is the number of elastic fuselage modes retained in the truncated modal model of the flexible fuselage.

The dominant components of the rotor loads, transmitted through the hub to the fuselage, are integer multiples of the rotor passage frequency $n_i N_b \Omega$. Therefore, the combined response of the fuselage, consisting of a combination of rigid body and elastic degrees of freedom, will contain primarily integer multiples of N_b/rev harmonics. In steady forward flight, a periodic solution in the form of Fourier series is assumed for the blade and fuselage degrees of freedom,[14,34] which can be expanded as follows:

$$\boldsymbol{q}_b = \boldsymbol{q}_{b_0} + \sum_{n=1}^{N_H} \left\{\boldsymbol{q}_{b_{\text{nc}}} \cos(n\psi) + \boldsymbol{q}_{b_{\text{ns}}} \sin(n\psi)\right\} \tag{29}$$

$$\boldsymbol{q}_r = \boldsymbol{q}_{r_0} + \sum_{n=1}^{N_{\text{rg}}} \left\{\boldsymbol{q}_{r_{\text{nc}}} \cos(nN_b\psi) + \boldsymbol{q}_{r_{\text{ns}}} \sin(nN_b\psi)\right\} \tag{30}$$

$$\boldsymbol{q}_e = \boldsymbol{q}_{e_0} + \sum_{n=1}^{N_{\text{el}}} \left\{\boldsymbol{q}_{e_{\text{nc}}} \cos(nN_b\psi) + \boldsymbol{q}_{e_{\text{ns}}} \sin(nN_b\psi)\right\} \tag{31}$$

The equations of motion represented by Eqs. (21–24) can be expressed explicitly in terms of Fourier series expansion coefficients by substituting into them Eqs. (29–31) and applying the harmonic balance technique to yield a system of nonlinear coupled algebraic equations. The resulting blade equations of motion expressed in terms of expansion coefficients can be symbolically represented as follows:

$$\boldsymbol{F}_b = \boldsymbol{F}_{b_0} + \sum_{n=1}^{N_H} \left\{\boldsymbol{F}_{b_{\text{nc}}} \cos(n\psi) + \boldsymbol{F}_{b_{\text{ns}}} \sin(n\psi)\right\} \tag{32}$$

where

$$\boldsymbol{F}_{b_0} = \frac{1}{2\pi}\int_0^{2\pi} \boldsymbol{F}_b(\boldsymbol{q}, \dot{\boldsymbol{q}}, \ddot{\boldsymbol{q}}, \boldsymbol{q}_t; \psi)\, \mathrm{d}\psi$$

$$\boldsymbol{F}_{b_{\text{nc}}} = \frac{1}{\pi}\int_0^{2\pi} \boldsymbol{F}_b(\boldsymbol{q}, \dot{\boldsymbol{q}}, \ddot{\boldsymbol{q}}, \boldsymbol{q}_t; \psi) \cos(n\psi)\, \mathrm{d}\psi$$

$$\boldsymbol{F}_{b_{\text{ns}}} = \frac{1}{\pi}\int_0^{2\pi} \boldsymbol{F}_b(\boldsymbol{q}, \dot{\boldsymbol{q}}, \ddot{\boldsymbol{q}}, \boldsymbol{q}_t; \psi) \sin(n\psi)\, \mathrm{d}\psi \tag{33}$$

Similar equations are obtained for the expansions of the fuselage rigid body and elastic equations of motion.

Table 1 Helicopter data

Parameter	Value
Soft in-blade data and frequencies for the four bladed rotor[a]	
C_W	0.005
σ	0.07
β_p	0.0
$fC_{d_f}/\pi R^2$	0.01
h_1/R	0.2851
h_2/R	0.2851
a	2π
c/R	0.055
$EI_y/m_b\Omega^2R^2$	0.0106
$EI_z/m_b\Omega^2R^2$	0.0301
$GJ/m_b\Omega^2R^2$	0.001473
ω_{F_1}	1.124
ω_{F_2}	3.407
ω_{F_3}	7.617
ω_{L_1}	0.7311
ω_{L_2}	4.453
ω_{T_1}	3.175
ω_{T_2}	9.097
Data for the complete three-dimensional elastic fuselage	
A/R^2	0.788×10^{-4}
$E/m_b\Omega^2$	0.662×10^{7}
$G/m_b\Omega^2$	0.249×10^{7}
$\rho/(m_b/R^2)$	0.119×10^{5}
I_x/R^4	0.193×10^{-8}
I_y/R^4	0.966×10^{-9}
I_z/R^4	0.966×10^{-8}
Elements	300
Degrees of freedom	966
Nodes	161

[a]The offsets of blade center of mass, aerodynamics center, and tension center from the elastic axis are zero.

Table 2 Fuselage mode shape frequencies

Mode shape description	Frequency, Hz
Fuselage yawing	5.28
Fuselage pitching	5.36
Fuselage torsion	11.07
Fuselage compression	18.81
Tail boom bending	23.23
Fuselage torsion	25.11
Landing gear vertical	26.73
Landing gear lateral	29.02

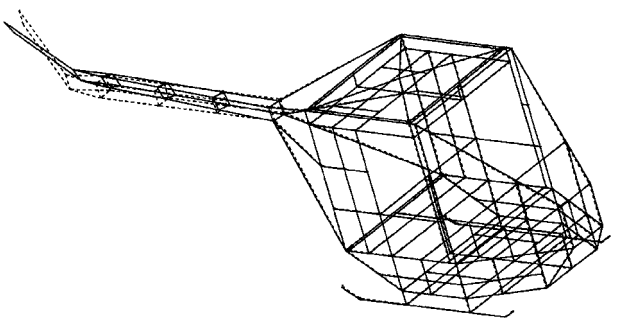

Fig. 5a Fuselage torsional mode; 11.07 Hz.

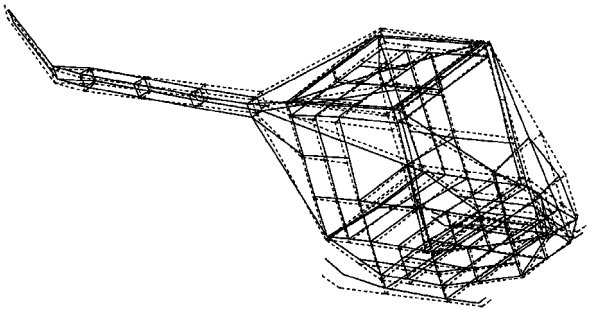

Fig. 5b Landing gear vertical mode; 26.73 Hz.

The rotor inertial, aerodynamic, gravitational, and damping loads are integrated along the blade span for each blade and combined at the hub. Subsequently, the loads are transformed to the nonrotating reference frame. These hub loads are input into the fuselage equations of motion so that exact rotor/fuselage coupling is enforced.

The set of trim, blade, fuselage rigid body, and fuselage elastic equations is combined and solved simultaneously for steady and level forward flight to yield the required solution vector. This system of equations is solved by the IMSL nonlinear algebraic equation solver, DNEQNF.[35] This routine uses the Levenberg–Marquardt algorithm to solve the trim and aeroelastic response simultaneously and calculates the Jacobian of the system using a finite difference scheme.

As described in the mathematical formulation of the wake model, the wake calculation routine returns influence matrices that relate the inflow distribution to the circulation distribution. However, the circulation distribution is dependent on the required lift, and the lift is dependent on the inflow distribution. Thus, it is necessary to iterate on circulation convergence for the prescribed wake and free wake iterations. Given the circulation distribution from the solution of the previous wake iteration, the inflow distribution is determined. From the inflow distribution, the distribution of lift is calculated. From the calculated lift, the required circulation is determined, and the process repeats until the circulation converges to within a prescribed limit.

For the correct calculation of the Jacobian in the IMSL routine DNEQNF, all parameters other than the specific one being varied

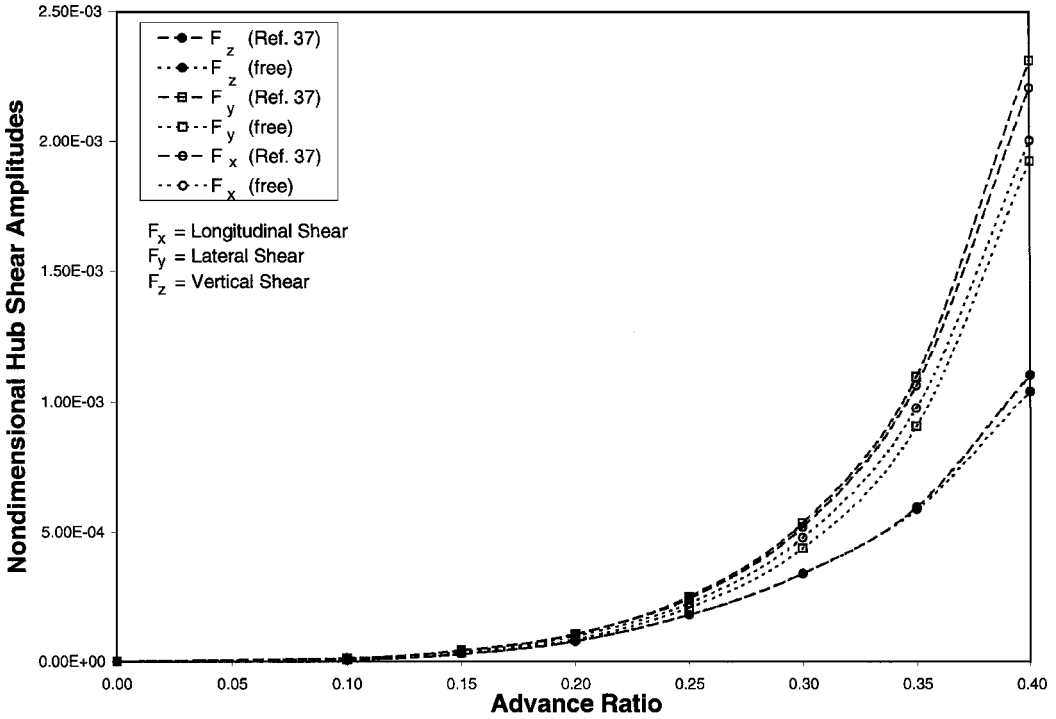

a) Hub shears

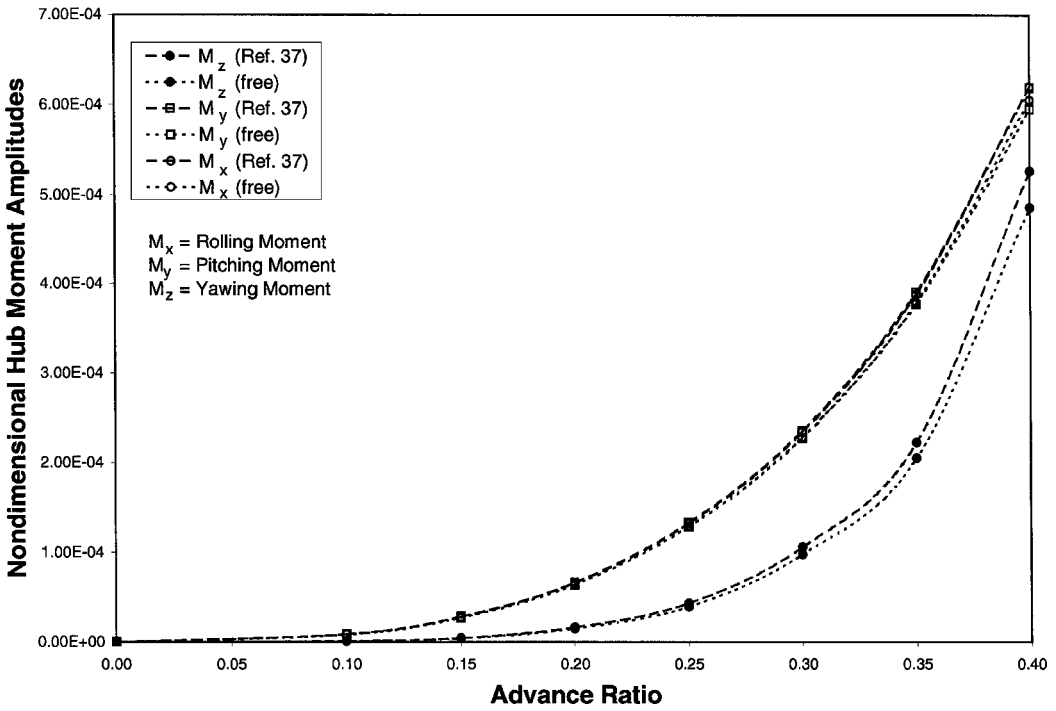

b) Hub moments

Fig. 6 Hub loads vs advance ratio.

must remain fixed. To keep the inflow distribution fixed, the circulation cannot vary. This requires a modification to the circulation iteration of CAMRAD/JA such that the circulation is not updated during the computation of the Jacobian. As a consequence, the circulation values near the blade tip converge slower than in the iterative procedure used in CAMRAD/JA, where the number of updates is greater. To remedy this situation, a test that checks the circulation convergence in the tip region has been added to the maximum bound circulation convergence test that CAMRAD/JA utilizes.

Convergence of the coupled trim/aeroelastic code requires a reasonable initial guess for the trim vector. For starting the uniform inflow iteration, the solution for hover, i.e., $\mu = 0$, is used as the initial guess for the values of forward flight solution, and the advance ratio is gradually incremented. It is noteworthy that the initial guesses for the fuselage rigid body and elastic degrees of freedom are not critical for convergence of the coupled rotor/fuselage code, and, therefore, they are set to zero for convenience.[36] Whereas the number of harmonics used in the expansion of blade displacements determines the accuracy of the results, the number has a minor effect on the rate of convergence of the coupled rotor/fuselage code. Similarly, the rate of convergence of the coupled rotor/fuselage problem is insensitive to the number of flexible modes retained in the fuselage model.[36] For the prescribed and free wake iterations, the solution vector from the preceding iteration is used as the initial guess.

After the trim and response solution vectors have been found, the rotor vibratory hub loads are determined. The loads at the root of

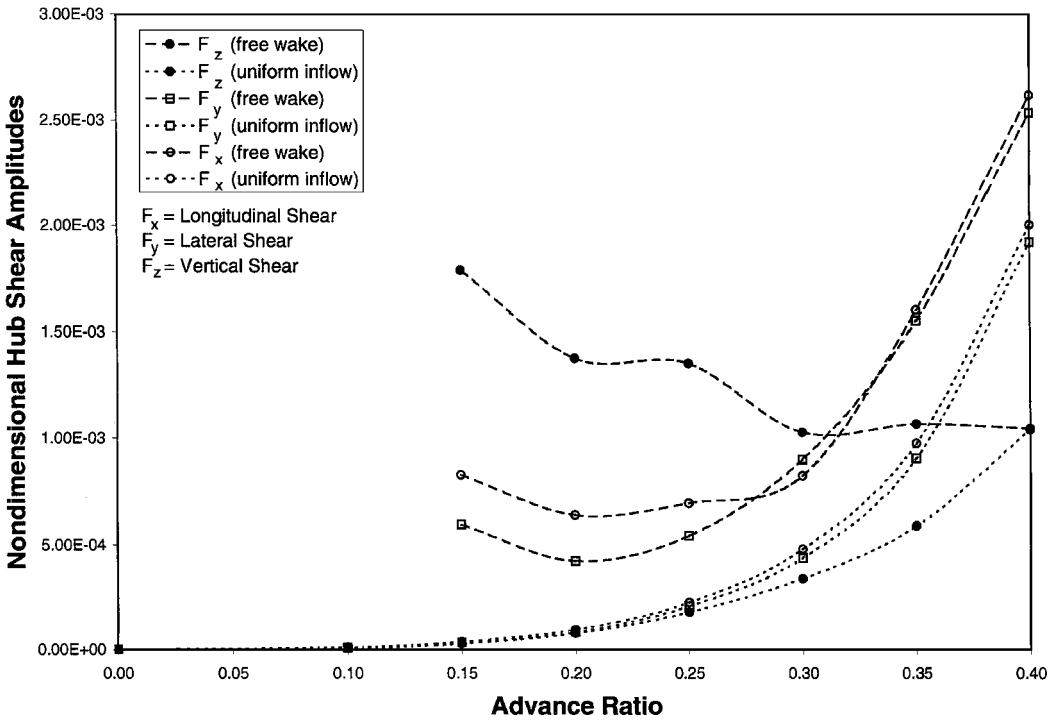

a) Hub shears

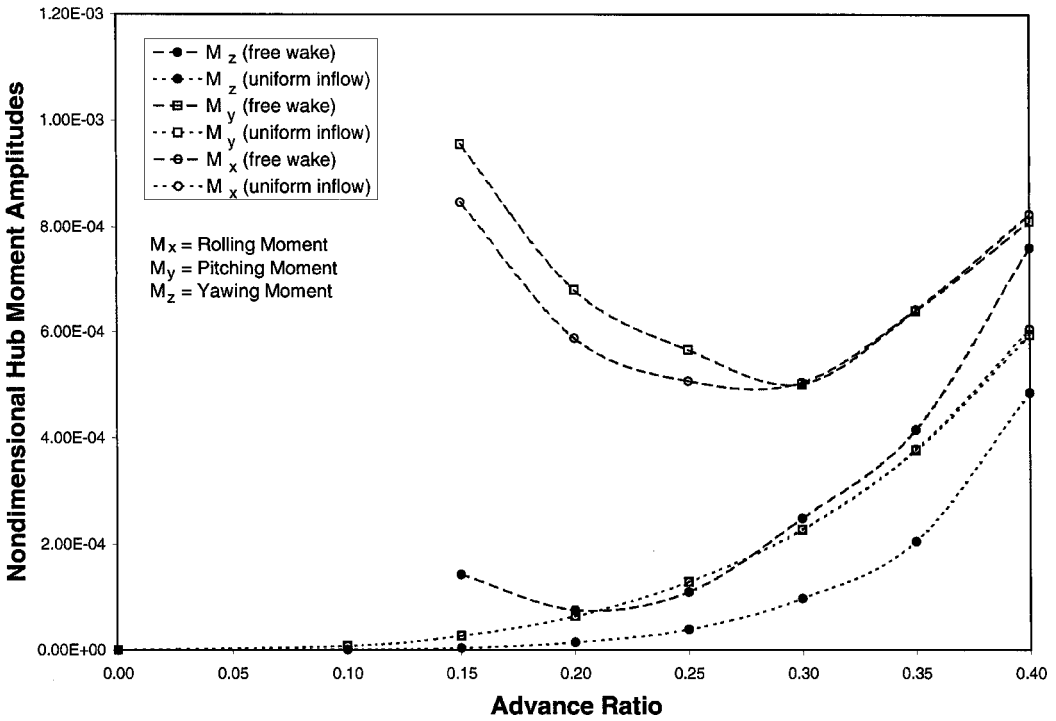

b) Hub moments

Fig. 7 Influence of aerodynamic model on vibratory hub loads.

the kth blade are obtained in the rotating frame by integrating the distributed loads along the span of the blade. These root loads are subsequently transferred to the hub and transformed to the hub fixed, nonrotating, reference frame. The summation of the contributions from the various blades yields the total vibratory hub loads. For an N_b-bladed rotor, the vibratory hub loads are primarily N_b/rev. In this study, the hub shear, moment, and acceleration vector amplitudes are defined, respectively, as follows:

$$|F| = \sqrt{F_{N_bC}^2 + F_{N_bS}^2}, \qquad |M| = \sqrt{M_{N_bC}^2 + M_{N_bS}^2}$$

$$|a| = \sqrt{a_{N_bC}^2 + a_{N_bS}^2} \tag{34}$$

where Eq. (34) corresponds to the oscillatory part of the hub loads and acceleration vectors given by

$$F_H = F_0 + F_{N_bC}\cos(N_b\psi) + F_{N_bS}\sin(N_b\psi)$$

$$M_H = M_0 + M_{N_bC}\cos(N_b\psi) + M_{N_bS}\sin(N_b\psi)$$

$$a_b = a_0 + a_{N_bC}\cos(N_b\psi) + a_{N_bS}\sin(N_b\psi) \tag{35}$$

Results and Discussion

In this section, the results for a coupled rotor/flexible fuselage model are presented for a four-bladed helicopter. The first eight fuselage free vibration modes and the comparison of the vibratory hub loads for the hub fixed and hub free cases are also presented. The helicopter parameters are chosen to model approximately an MBB BO-105 helicopter operating at a weight coefficient of $C_w = 0.005$, with soft-in-plane hingeless rotor blades. The three-dimensional fuselage is modeled by beam elements combined with nonstructural masses, as depicted in Fig. 1.

For the soft-in-plane rotor, the basic data used in the computation, together with the uncoupled rotating natural frequencies for the blade modes, are given in Table 1. The chosen airfoil is the NACA 0012. All calculations were carried out using seven modes for each blade: three flap, two lag, and two torsional modes. Six harmonics were used in generating the blade responses. The data for the finite element representation of the fuselage are also provided in Table 1. The flexible fuselage dynamics are represented by a truncated set of eight natural modes of free vibration, so as to reduce the number of degrees of freedom associated with fuselage flexibility. It should also be mentioned that the comparison studies described in Ref. 36 have verified the reliability of the aeroelastic response code for the fixed hub case; because of lack of space, these results are not shown in this paper.

Fuselage Free Vibration Modes

The frequencies of the first eight elastic free vibration modes are provided in Table 2. It should be emphasized that the identification of these modes by the descriptive terms in the table is qualitative. In reality, these are all coupled modes, and their qualitative identification is associated with the principal contribution of the degrees of freedom mentioned in the overall motion of the fuselage. Mode shapes for two of the modes are provided in Fig. 5.

Comparison of Coupled Rotor/Flexible Fuselage and Hub Fixed Results

To assess the effects of fuselage coupling on the helicopter hub loads, the hub shears and moments of the fully coupled rotor/flexible fuselage model are compared with the corresponding values of the hub fixed case assuming a uniform inflow. The hub fixed results are taken from Ref. 37, which uses the same rotor model as the current study. Figures 6a and 6b depict the hub loads as a function of advance ratio for both the hub fixed and hub free cases. Figure 6a indicates that the hub shears generated with the hub fixed assumption are slightly higher than the corresponding hub free values. Similar observations can be made regarding the hub moments as illustrated in Fig. 6b. Thus, the inclusion of the flexible fuselage has a minor effect on rotor hub loads.

Uniform Inflow and Free Wake Results Comparison

The importance of a refined aerodynamic model on the 4/rev vibratory hub loads of a four-bladed helicopter is shown in Figs. 7a and 7b. Both figures present the hub loads as a function of advance ratio for both the uniform inflow and free wake models. Figure 7a shows the powerful effect of the inclusion of a free wake model on the 4/rev hub shears. These vibratory hub shears are significantly higher with the refined aerodynamic model, especially at lower advance ratios where blade vortex interaction plays a larger role. The differences between the results of the two aerodynamic models diminish at higher advance ratios. As illustrated by Fig. 7b, the vibratory hub moments have similar characteristics. These figures show

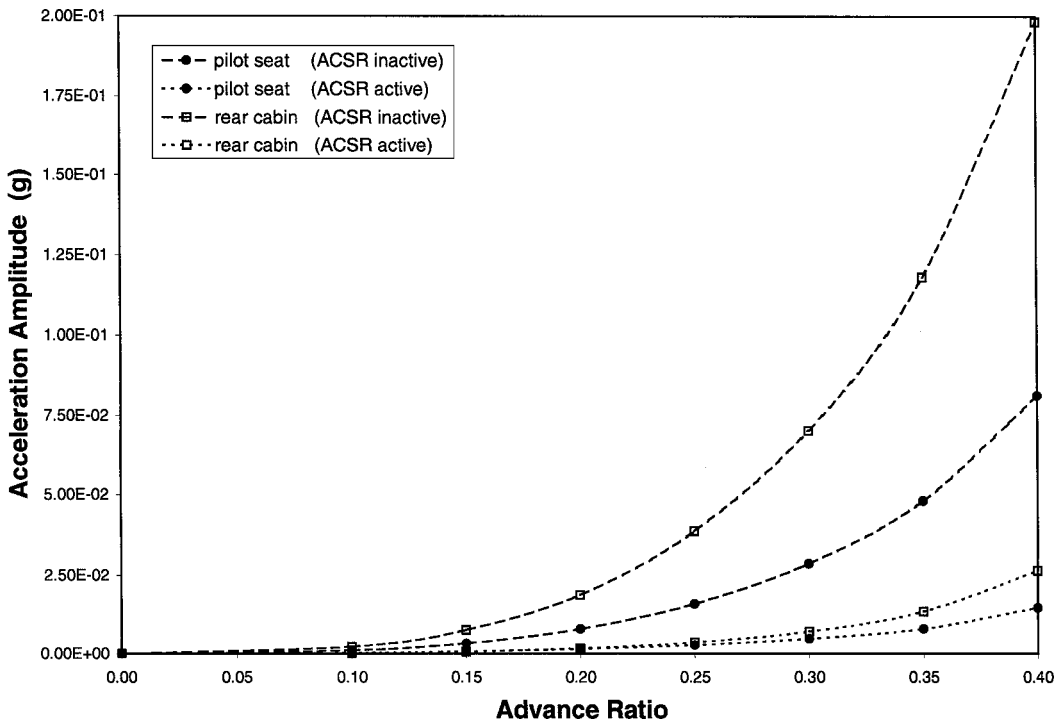

Fig. 8 Uniform inflow accelerations for ACSR: active and inactive.

the necessity of including refined aerodynamic models in the calculation of vibratory hub loads and, therefore, in the calculation of fuselage acceleration levels.

Vibration Reduction Using ACSR

As stated in the introduction, the purpose of the described analytical model is to investigate the vibration reduction capabilities of ACSR. To demonstrate this capability, Figs. 8–11 provide sample results from an ACSR simulation. The full set of results are to be presented in a later paper. The control algorithm used in this simulation is described by Chiu and Friedmann.[38] In this scheme, the forces across the servo actuators, due to control inputs and spring forces due to fuselage elastic deformation, are set to zero through the proper choice of control inputs. Figure 8 shows the vertical acceleration levels at the pilot seat and at a rear cabin position of a four-bladed helicopter, assuming uniform inflow for both cases of the controller active and inactive. The vibrations at the rear cabin position are greater than those at the pilot seat. As seen in the figure, the vibration levels at both locations are markedly reduced by the ACSR system. This vibration reduction is evident at all advance ratios. The amplitudes of the oscillatory actuator forces required for this vibration reduction are shown in Fig. 9. For the uniform inflow model, the required actuator forces increase as advance ratio increases. At an advance ratio of 0.4, actuators capable of producing forces on the order of 2500 lb (11,125 N) are required. Figure 10 depicts the vertical acceleration levels of the same four-bladed helicopter using the free wake model. The ACSR system reduces vibration levels also in this case. The actuator requirements for the free wake model are shown in Fig. 11. With the free wake model, large actuator forces are required at lower advance ratios where the vibratory hub loads are much higher than in the uniform inflow model. The ACSR system requires forces on the order of 4000 lb (17,800 N) for this aerodynamic model. With both aerodynamic models, the power required by the ACSR system is less than 1% of the total rotor power for all advance ratios

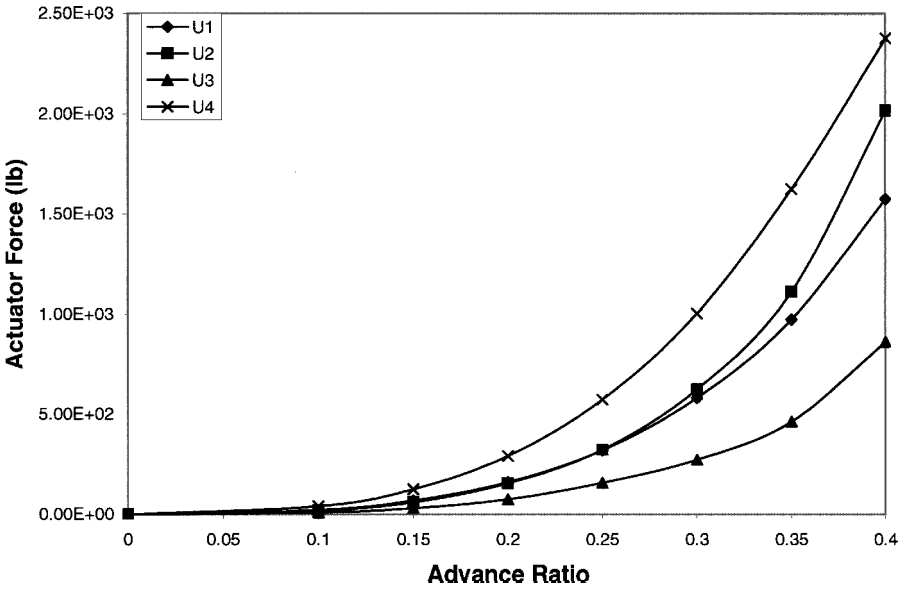

Fig. 9 Uniform inflow actuator force amplitudes.

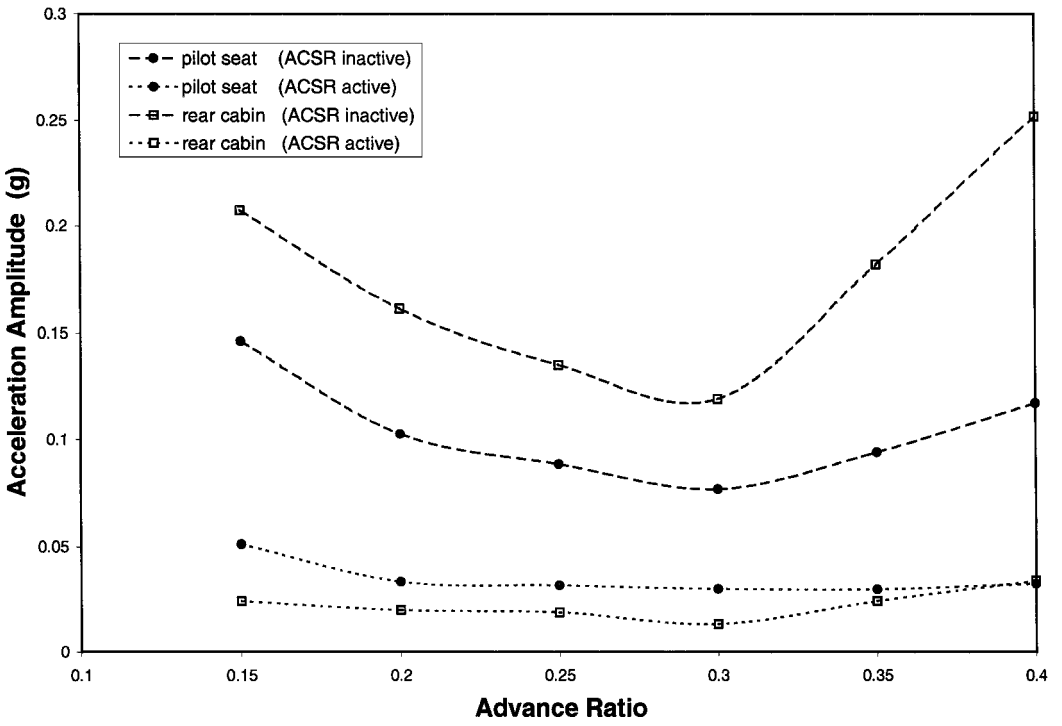

Fig. 10 Free wake accelerations for ACSR: active and inactive.

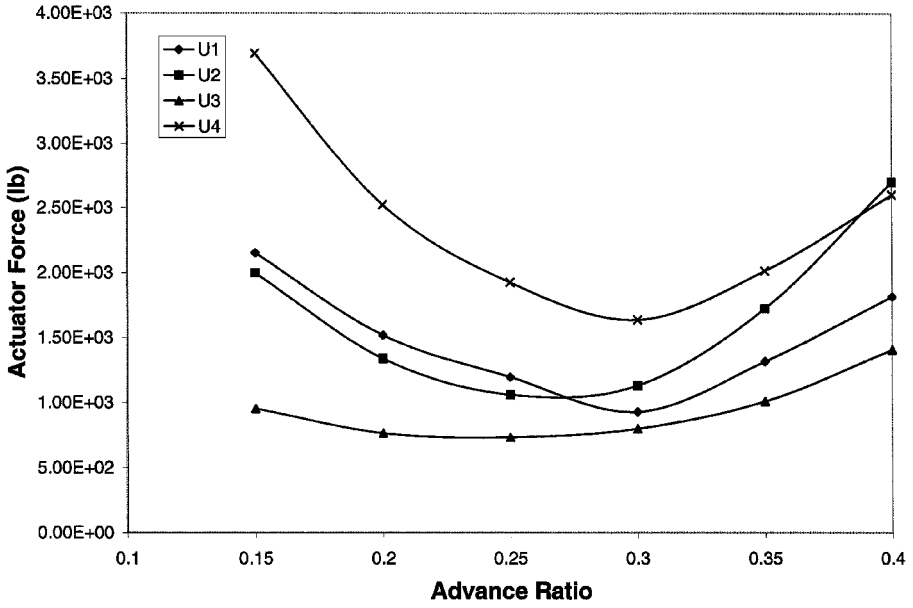

Fig. 11 Free wake actuator force amplitudes.

but is higher for the free wake model than for the uniform inflow model.

Conclusions

A refined coupled rotor/flexible fuselage model, which also contains a provision for modeling a novel type of vibration suppression device denoted by the term ACSR, combined with a free wake model, has been derived and implemented in an aeroelastic response analysis code. The rotor is represented by hingeless blades, while the fuselage is represented by a three-dimensional finite element model, which model also includes the important effects of nonstructural masses. The approach combines a nonlinear rotor model, where the nonlinearities are due to moderate blade deflections, with a linear modal representation of the flexible fuselage.

The aerodynamic model of the wake has a significant impact on the vibratory hub loads. The results obtained using uniform inflow show markedly lower levels of vibratory hub shears and moments than those obtained with the free wake model. These differences are most notable at those lower advance ratios where blade vortex interactions play a larger role.

The study also indicates that the accelerations at various fuselage locations considered are dependent on the locations where they are measured, with the accelerations higher for the rear cabin location than the pilot seat. The ACSR system is able to reduce these accelerations at all advance ratios. The actuator force and power requirements for ACSR are higher for the free wake model than for the uniform inflow model. The power required is less than 1% of the total rotor power for both aerodynamic models.

An aeroelastic response model such as described in this paper is a valuable tool for conducting actively controlled vibration studies using the ACSR system.

Acknowledgments

This research was supported by the U.S. Army Research Office under Grants DAA H04-93-G-0004 and DAA H04-95-I-0320, with Gary Anderson as Technical Monitor.

References

[1]Crews, S. T., "Rotorcraft Vibration Criteria: A New Perspective," *Proceedings of the 43rd Annual Forum of the American Helicopter Society*, American Helicopter Society, Alexandria, VA, 1987, pp. 991–998.

[2]*Aeronautical Design Standard (ADS-27)*; *Requirements for Rotorcraft Vibration Specifications, Modeling, and Testing*. U.S. Army Aviation System Command, 1986.

[3]Reichert, G., "Helicopter Vibration Control—A Survey," *Vertica*, Vol. 5, No. 1, 1981, pp. 1–20.

[4]Loewy, G. R., "Helicopter Vibrations: A Technological Perspective," *Journal of the American Helicopter Society*, Vol. 29, No. 4, 1984, pp. 4–30.

[5]Kvaternik, R. G., Bartlett, F. D., Jr., and Cline, J. H., "A Summary of Recent NASA/ARMY Contributions to Rotorcraft Vibrations and Structural Dynamics Technology," NASA CP-2495, 1988.

[6]Friedmann, P. P., and Millott, T. A., "Vibration Reduction in Rotorcraft Using Active Control: A Comparison of Various Approaches," *Journal of Guidance, Control, and Dynamics*, Vol. 18, No. 4, 1995, pp. 664–673.

[7]King, S. P., and Staple, A. E., "Minimization of Helicopter Vibration Through Active Control of Structural Response," *Rotorcraft Design Operations*, CP-423, AGARD, Oct. 1986, pp. I4–1–I4–13.

[8]Staple, A. E., "An Evaluation of Active Control of Structural Response as a Means of Reducing Helicopter Vibration," *Proceedings of the 15th European Rotorcraft Forum*, National Aerospace Lab. NLR, Amsterdam, 1989, pp. 3–17.

[9]Welsh, W. A., von Hardenberg, P. C., von Hardenberg, P. W., and Staple, A. E., "Test and Evaluation of Fuselage Vibration Utilizing Active Control of Structural Response (ACSR) Optimized to ADS-27," *Proceedings of the 46th Annual Forum of the American Helicopter Society*, American Helicopter Society, Alexandria, VA, 1990, pp. 21–37.

[10]Niwa, Y., and Katayama, N., "Active Vibration Reduction System for a Helicopter," *Proceedings of the 20th European Rotorcraft Forum*, National Aerospace Lab. NLR, Amsterdam, 1994, pp. 70-01–70-14.

[11]Kawaguchi, H., Bandoh, S., and Niwa, Y., "The Test Results for AVR (Active Vibration Reduction) System," *Proceedings of the 52nd Annual Forum of the American Helicopter Society*, American Helicopter Society, Alexandria, VA, 1996, pp. 123–136.

[12]Venkatesan, C., and Friedmann, P., "Aeroelastic Effects in Multi-Rotor Vehicles with Applications to a Heavy-Lift System, Part 1: Formulation of Equations of Motion," NASA CR-3822, Aug. 1984.

[13]Venkatesan, C., and Friedmann, P., "Aeroelastic Effects in Multi-Rotor Vehicles, Part 2: Method of Solution and Results Illustrating Coupled Rotor-Fuselage Aeromechanical Stability," NASA CR-4009, Feb. 1987.

[14]Papavassiliou, I., Friedmann, P. P., and Venkatesan, C., "Coupled Rotor/Fuselage Vibration Reduction Using Open-Loop Blade Pitch Control," *Mathematical Computer Modeling*, Vol. 18, No. 3, 1993, pp. 131–156.

[15]Vellaichamy, S., and Chopra, I., "Aeroelastic Response of Helicopters with Flexible Fuselage Modeling," *Proceedings of the 33rd AIAA/ASME/ASCE/AHS/ASC Structures, Structural Dynamics, and Materials Conference*, AIAA, Washington, DC, 1992, pp. 2015–2026.

[16]Vellaichamy, S., and Chopra, I., "Effect of Modeling Techniques in the Coupled Rotor-Body Vibration Analysis," *Proceedings of the 34th AIAA/ASME/ASCE/AHS/ASC Structures, Structural Dynamics, and Materials Conference*, AIAA, Washington, DC, 1993, pp. 563–575.

[17]Yeo, H., and Chopra, I., "Modeling Issues Related to Vibration Prediction of a Coupled Rotor/Fuselage System," *Proceedings of the 38th AIAA/ASME/ASCE/AHS/ASC Structures, Structural Dynamics, and Materials Conference*, AIAA, Reston, VA, 1997, pp. 2739–2751.

[18]Yeo, H., and Chopra, I., "Effects of Modeling Refinements on Couple Rotor/Fuselage Vibration Analysis," *Proceedings of the 54th Annual Forum of the American Helicopter Society*, American Helicopter Society, Alexandria, VA, 1998, pp. 489–501.

[19]Rosen, A., and Friedmann, P. P., "Nonlinear Equations of Equilibrium for Elastic Helicopter or Wind Turbine Blades Undergoing Moderate Deformation," NASA CR-159478, Dec. 1978.

[20]*MACSYMA: Reference Manual*, Symbolics, Arlington, MA, 1986.

[21]Greenberg, J. M., "Airfoil in Sinusoidal Motion in a Pulsating Stream," NACA TN-1326, 1947.

[22]Shamie, J., and Friedmann, P. P., "Effect of Moderate Deflections on the Aeroelastic Stability of a Rotor Blade in Forward Flight," *Proceedings of the 3rd European Rotorcraft and Powered Lift Aircraft Forum*, Association Aeronautique et Astronautique de France, Sept. 1977, pp. 24-1–24-37.

[23]Friedmann, P. P., "Rotary-Wing Aeroelasticity with Application to VTOL Vehicles," *Proceedings of the 31st AIAA/ASME/ASCE/AHS/ASC Structures, Structural Dynamics, and Materials Conference*, AIAA, Washington, DC, 1990, pp. 1624–1670.

[24]Johnson, W., *A Comprehensive Analytical Model of Rotorcraft Aerodynamics and Dynamics*, *Vol. I: Theory Manual*, Johnson Aeronautics, Palo Alto, CA, 1988.

[25]Johnson, W., *A Comprehensive Analytical Model of Rotorcraft Aerodynamics and Dynamics*, *Vol. II: User's Manual*, Johnson Aeronautics, Palo Alto, CA, 1988.

[26]Scully, M. P., "Computation of Helicopter Rotor Wake Geometry and Its Influence on Rotor Harmonic Airloads," Ph.D. Dissertation, Aeroelastic Research Lab., Massachusetts Inst. of Technology, Cambridge, MA, 1975.

[27]Johnson, W., "Wake Model for Helicopter Rotors in High Speed Flight," NASA CR-177507, Nov. 1988.

[28]Milne, R. D., "Dynamics of the Deformable Aeroplane," Her Majesty's Stationery Office, Reports and Memoranda 3345, Sept. 1962.

[29]Waszak, M. R., and Schmidt, D. K., "Flight Dynamics of Aeroelastic Vehicles," *Journal of Aircraft*, Vol. 23, No. 6, June 1988, pp. 563–571.

[30]Shames, I. H., and Dym, C. L., *Energy and Finite Element Methods in Structural Mechanics*, Taylor and Francis, Washington, DC, 1985, pp. 112–143.

[31]Surana, K., "Consistent Mass Matrices for Three Dimensional Beam Element Due to Distributed and Lumped Non-Structural Mass Systems Acting on Its Span," *Computers and Structures*, Vol. 13, 1981, pp. 515–524.

[32]Stoppel, J., and Degener, M., "Investigations of Helicopter Structural Dynamics and a Comparison with Ground Vibration Tests," *Journal of the American Helicopter Society*, Vol. 27, April 1982, pp. 34–42.

[33]Zienkiewicz, O. C., *The Finite Element Method*, 4th ed., Vol. 2, McGraw–Hill, New York, 1991.

[34]Millott, T. A., and Friedmann, P. P., "Vibration Reduction in Helicopter Rotors Using an Active Control Surface Located on the Blade," *Proceedings of the 33rd AIAA/ASME/ASCE/AHS/ASC Structures, Structural Dynamics, and Materials Conference*, AIAA, Washington, DC, 1992, pp. 1975–1988.

[35]International Mathematical and Statistical Library, *IMSL Library: Reference Manual*, Houston, TX, 1980.

[36]Chiu, T., and Friedmann, P. P., "A Coupled Helicopter Rotor-Fuselage Aeroelastic Response Model for ACSR," *Proceedings of the 36th AIAA/ASME/ASCE/AHS/ASC Structures, Structural Dynamics, and Materials Conference*, AIAA, Washington, DC, 1995, pp. 574–600.

[37]Millott, T. A., and Friedmann, P. P., "Vibration Reduction in Helicopter Rotors Using an Actively Controlled Partial Span Trailing Edge Flap Located on the Blade," NASA CR-4611, June 1994.

[38]Chiu, T., and Friedmann, P. P., "ACSR System for Vibration Suppression in Coupled Rotor-Flexible Fuselage Model," *Proceedings of the 37th AIAA/ASME/ASCE/AHS/ASC Structures, Structural Dynamics, and Materials Conference*, AIAA, Reston, VA, 1996, pp. 1972–1991.

A. Plotkin
Associate Editor